INTERNATIONAL JOURNAL FOR NUMERICAL METHODS IN ENGINEERING, VOL. 20, 2311–2324 (1984)

THE POST-PROCESSING APPROACH IN THE FINITE ELEMENT METHOD—PART 3: *A POSTERIORI* ERROR ESTIMATES AND ADAPTIVE MESH SELECTION†

I. BABUŠKA AND A. MILLER

Institute for Physical Science and Technology, University of Maryland, College Park, Maryland, U.S.A.

SUMMARY

This paper is the final in a series of three in which we have discussed a finite element post-processing technique. Here we shall deal with the questions of adaptive mesh selection and *a posteriori* error estimation. Some numerical examples computed by the FEARS program will be used to illustrate the approaches taken.

1 INTRODUCTION

This is the final in a series of three papers in which we have sought to show how a suitable post-processing of a finite element solution can yield accurate pointwise values for quantities such as displacements, stresses, flow rates and stress intensity factors. In References 1 and 2 we derived a number of extraction expressions for such quantities in the setting of some simple model problems, and saw how these expressions could serve as the bases of effective post-processing techniques. We also carried out an error analysis for such post-processing computations. This analysis showed that the accuracy of the post-processed value could be related to how well the space of finite element functions is able to approximate both the solution of the basic problem and the solution of a related auxiliary problem. This auxiliary problem is of the same form as the basic problem, although with different loading data. (See Subsections 2.5 and 3.4 of Reference 1, and Section 4 of Reference 2.)

Hitherto, except for a few qualitative remarks, we have said little concerning the issues of (a) choosing a finite element subspace for calculating the approximate solution which is to be subsequently post-processed, and (b) estimating, *a posteriori*, the error in a computed post-processed value.

The significance of both (a) and (b) is quite clear. In practice, the goal of any post-processing computation is to obtain a post-processed value of a specified accuracy at a minimal total computational cost. An estimate as in (b) provides a means of determining when the specified accuracy has been attained, whereas the choice in (a) largely determines the efficiency of the overall numerical procedure.

In this paper we propose a post-processing algorithm. It is based on the extraction techniques of References 1 and 2, and includes features that enable (a) and (b) to be handled quite effectively. Our discussion will be in the context of the 'membrane' model problems already introduced in Section 5 of Reference 1 and Section 6 of Reference 2. In these, the order of

† This research was partially supported by ONR Contract N00014-77-C-0623. The computations were carried out with support from the Computer Science Center at the University of Maryland, College Park, MD, U.S.A.

0029–5981/84/122311–14$01.40 *Received 17 June 1983*

the elements employed is fixed (square bilinear elements are used), and (a) becomes a matter of choosing a finite element mesh (i.e. nodal points). The manner in which we realize (a) and (b) will make use of some of the features available in the FEARS program. In Section 2 of this paper, we briefly describe the relevant features of FEARS. In Subsection 3.1, we review the error analysis of our earlier papers[1,2] and show how this analysis suggests some *a posteriori* error estimates that can be computed within the FEARS framework. These *a posteriori* estimates are the basis of the proposed algorithm, which we describe in Subsection 3.2. Finally, in Section 4, we return to some of the numerical examples of Section 5 of Reference 1 and Section 6 of Reference 2, this time concentrating on some new aspects which are related to the issues (a) and (b).

2 THE FEARS PROGRAM

FEARS is a research oriented, adaptive finite element code developed at the University of Maryland. A detailed description of the operation of the program can be found in Reference 3. For the purposes of this paper, the following few remarks will suffice. As already explained in Reference 2, FEARS assumes that the region under consideration has first been partitioned into a number of subregions, each of which is a curvilinear quadrilateral. Within the program, each of these subregions is transformed by a change of co-ordinates into a unit square. The actual finite element modelling is carried out on these transformed squares. Square bilinear elements are used. FEARS has an adaptive character: starting from an initial coarse mesh (usually uniform on each of the transformed squares), the program automatically selects, in a recursive fashion, a sequence of 'optimal' mesh refinements.

The mesh refinement procedure is based upon a set of non-negative error indicators. An indicator, η_Δ say, is associated with each element Δ. It is calculated only using information about the finite element solution on Δ itself and on the immediately adjacent elements. These error indicators, when summed over all elements to obtain

$$\varepsilon = \sum_{\substack{\text{all elements} \\ \Delta}} \eta_\Delta \tag{1}$$

say, yield an estimate for some user specified measure of the error in the finite element solution. Typically, this measure is closely related to the energy of the error. (Later we shall say a little more—see Sections 3 and 4.) Each step in the refinement process is directed towards minimizing the sum ε of (1) in some 'optimal' fashion. To this end, all elements Δ of an existing mesh whose error indicators η_Δ exceed a threshold value are subdivided. This threshold is determined from some information on the past history of the refinement process. Of course, the character of the meshes constructed by FEARS will depend upon which error measure has been specified. This reflects the fact that the quality of a mesh is not an absolute property, but must be viewed relative to the ultimate goal of the finite element calculation. We shall elaborate further upon the point in Section 4.

In FEARS, the finite element equations are solved by a direct method. Usually, after each refinement step a full new solution is calculated and a new set of error indicators is found. However, calculating a new solution each time is quite expensive, and as it is just an intermediate step, only being used to compute the new error indicators for the next refinement step, one would like to avoid it, if possible. FEARS has a number of 'economy' modes which do this to varying degrees. In these, a full solution is computed only after a specified increase in the total number of elements has occurred since the last full solution. After any refinement step between

two such full solution phases, the new error indicators are only approximated on the basis of the past history of the local refinement process. This 'economy' mode permits a multi-level refinement to take place between two full solutions. This possibility is particularly desirable for efficient operation for problems with severe singularities. Provided the number of such 'short passes' between full solution steps is not too great, the resulting refinement pattern does not differ too much from that obtained by the all full solution method, but, of course, with a considerable saving in computational cost.

Estimates such as ε of (1), as well as being the basis of the automatic mesh refinement feature of FEARS, also provide a means of *a posteriori* error estimation. Of course, we cannot expect that the estimate ε should yield the exact value of the specified error measure. However, under suitable assumptions, estimates may be calculated that are asymptotically exact. That is, if e denotes the exact value of the desired error measure, then

$$e = \varepsilon(1 + o(1)) \quad \text{as } \varepsilon \to 0$$

To illustrate some of the points made above, let us return to Example A in Section 6 of Reference 2. In that example, we considered the boundary value problem

$$\begin{aligned} \nabla^2 \omega &= 0 && \text{in } \Omega \\ \omega &= 0 && \text{on } \Gamma_1 \\ \frac{\partial \omega}{\partial n} &= 0 && \text{on } \Gamma_2 \\ \frac{\partial \omega}{\partial n} &= x_2 && \text{on } \Gamma_3 \end{aligned} \tag{2}$$

where Ω is the unit circle slit along the positive x_1 axis and Γ_1, Γ_2 and Γ_3 are as shown in Figure 1. In Reference 2, we reported on a sequence of five adaptively refined meshes that FEARS constructed for this problem (see Subsection 6.2 of Reference 2). We can now be more specific. The mesh refinement process for this example relied upon error indicators η_Δ for which the sum ε of (1) is an asymptotically exact estimate for the strain energy measure $e = \int_\Omega |\nabla(\omega - \tilde{\omega})|^2 \, dA$ of the error in the finite element solution $\tilde{\omega}$. As we saw in Reference 2, the meshes so constructed yield a rate of convergence for the strain energy norm $e^{1/2}$ of the error that is close to the theoretically optimal rate of $O(N^{-1/2})$, where N is the number of degrees-of-freedom of the finite element model. In contrast, uniform meshes would only give

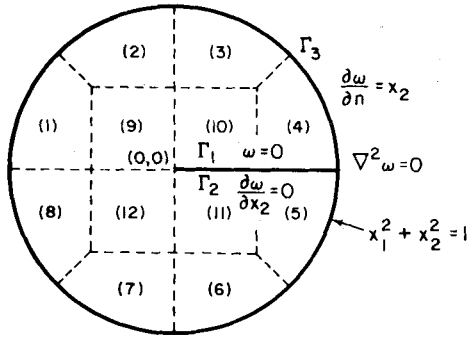

Figure 1. The region for the model problem (2)

Table I. *A posteriori* estimates of the error in the energy norm $e^{1/2}$ for the example of Section 2. ($E(\omega) = \int_\Omega |\nabla\omega|^2 \, dA$)

Mesh label (degrees-of-freedom)	$e^{1/2}$ true error norm ($e^{1/2}/E(\omega)^{1/2}$)	$\varepsilon^{1/2}$ estimated error norm	$\frac{\varepsilon^{1/2}}{e^{1/2}}$
I (56)	0·6577 (30·9%)	0·3747	0·57
II (89)	0·5156 (24·2%)	0·3544	0·69
III (118)	0·3875 (18·2%)	0·3108	0·80
IV (171)	0·2622 (12·3%)	0·2434	0·93
V (391)	0·1618 (7·6%)	0·1638	1·01

an $O(N^{-1/8})$ rate. In Table I we have listed $e^{1/2}$ and $\varepsilon^{1/2}$ for each of our meshes. Notice the $\varepsilon^{1/2}/e^{1/2}$ appears to be converging to 1, as it should, since ε is an asymptotically exact estimate for e. For this problem, FEARS was executed in an 'economy' mode, so permitting multi-level refinements between full solutions (the meshes I–V that we have referred to here and in Section 2 are a selection of meashes created by full solution steps). The efficiency of the 'economy' mode can be gauged by the fact that the total solution time for mesh V and all earlier full solutions was only about 2·5 times the solution time for mesh V alone.

3.1 A posteriori error estimates

For the model problems discussed in Section 5 of Reference 1 and in Reference 2, we saw that the difference between the exact value Φ of some quantity (e.g. displacement, stress, stress intensity factor) associated with the exact solution ω of a problem and an approximate value $\tilde{\Phi}$ obtained by suitably post-processing the finite element solution $\tilde{\omega}$ could be expressed as

$$\Phi - \tilde{\Phi} = \int_\Omega \nabla(\omega - \tilde{\omega}) \, . \, \nabla(\psi - \tilde{\psi}) \, dA \tag{3}$$

where ψ and $\tilde{\psi}$ are the exact and finite element solutions, respectively, of an auxiliary problem. This auxiliary problem is of the same form as the basic problem for ω, although with different loading data. The loading data is determined by the particular extraction functions used in the post-processing calculations.

For any function u, let $E(u)$ denote the 'membrane' strain energy of u,

$$E(u) = \int_\Omega |\nabla u|^2 \, dA$$

After a little algebraic manipulation (3) may be rewritten as

$$\Phi - \tilde{\Phi} = \tfrac{1}{4}[E((\omega + \psi) - (\tilde{\omega} + \tilde{\psi})) - E((\omega - \psi) - (\tilde{\omega} - \tilde{\psi}))] \tag{4}$$

Furthermore, the following inequalities also follow from (3),

$$|\Phi-\tilde{\Phi}| \leq E(\omega-\tilde{\omega})^{1/2}E(\psi-\tilde{\psi})^{1/2} \tag{5a}$$

$$|\Phi-\tilde{\Phi}| \leq \frac{1}{2\alpha}(E(\omega-\tilde{\omega})+\alpha^2 E(\psi-\tilde{\psi})) \tag{5b}$$

for any real number $\alpha > 0$. Notice that whereas (4) is an exact expression for the error $\Phi-\tilde{\Phi}$, in general (5a) and (5b) only yield upper bounds for $|\Phi-\tilde{\Phi}|$. They fail to take account of any cancellation in the integral (3). The inequality (5a) becomes an equality only if $(\omega-\tilde{\omega})$ and $(\psi-\tilde{\psi})$ are multiples of one another. (The inequality (5b) is a equality only in the more particular case $(\omega-\tilde{\omega}) = \pm\alpha(\psi-\tilde{\psi})$.) One way to think of this cancellation phenomenon is in terms of the 'angle' between the errors $(\omega-\tilde{\omega})$ and $(\psi-\tilde{\psi})$. Let γ be the angle lying between 0 and 90 degrees for which

$$\cos\gamma = \frac{|\int_\Omega \nabla(\omega-\tilde{\omega}) \,.\, \nabla(\psi-\tilde{\psi})\, dA|}{E(\omega-\tilde{\omega})^{1/2}E(\psi-\tilde{\psi})^{1/2}} \tag{6}$$

Then, $\gamma = 0$ degrees ($\cos\gamma = 1$) corresponds to the case for which (5a) is an equality, while $\gamma = 90$ degrees ($\cos\gamma = 0$) indicates complete cancellation in the integral (3). Continuing the geometrical analogy, we could say that in the case $\gamma = 0$ degrees, the errors $(\omega-\tilde{\omega})$ and $(\psi-\tilde{\psi})$ are 'parallel', and in the case $\gamma = 90$ degrees they are 'perpendicular'.

Means of estimating the quantities appearing on the right-hand sides of (4) and (5) are available in FEARS. If $\tilde{u}$ is the finite element solution of a problem whose exact solution is u, let $\varepsilon^0(\tilde{u}) = \sum_\Delta \eta_\Delta^0(\tilde{u})$ be an asymptotically exact estimate for $E(u-\tilde{u})$ which is constructed from elementary error indicators $\eta_\Delta^0(\tilde{u})$. That is,

$$E(u-\tilde{u}) = \varepsilon^0(\tilde{u})(1+o(1)) \quad \text{as } E(u-\tilde{u}) \to 0$$

So, (4) gives

$$\Phi-\tilde{\Phi} = \tfrac{1}{4}[\varepsilon^0(\tilde{\omega}+\tilde{\psi}) - \varepsilon^0(\tilde{\omega}-\tilde{\psi})] + o(1)[\varepsilon^0(\tilde{\omega}+\tilde{\psi}) + \varepsilon^0(\tilde{\omega}-\tilde{\psi})] \tag{7}$$

and (5) leads to

$$|\Phi-\tilde{\Phi}| \leq \varepsilon^0(\tilde{\omega})^{1/2}\varepsilon^0(\tilde{\psi})^{1/2}(1+o(1)) \tag{8a}$$

$$|\Phi-\tilde{\Phi}| \leq \frac{1}{2\alpha}(\varepsilon^0(\tilde{\omega})+\alpha^2\varepsilon^0(\tilde{\psi}))(1+o(1)) \tag{8b}$$

where the $o(1)$ term is valid as $E(\omega-\tilde{\omega})+E(\psi-\tilde{\psi}) \to 0$.

Equation (7) suggests that the quantity

$$\varepsilon_1 = \tfrac{1}{4}[\varepsilon^0(\tilde{\omega}+\tilde{\psi}) - \varepsilon^0(\tilde{\omega}-\tilde{\psi})] \tag{9}$$

should provide a good estimate for the error $\Phi-\tilde{\Phi}$, provided the $o(1)$ term is negligible. However, if the $o(1)$ term in (7) is comparable to

$$\mu = \frac{\tfrac{1}{4}[\varepsilon^0(\tilde{\omega}+\tilde{\psi}) - \varepsilon^0(\tilde{\omega}-\tilde{\psi})]}{\varepsilon^0(\tilde{\omega}+\tilde{\psi}) + \varepsilon^0(\tilde{\omega}-\tilde{\psi})}$$

then ε_1 is no longer reliable. In cases where the angle γ defined in (6) is close to 90 degrees, then μ may be quite small and ε_1 could well perform poorly. Turning now to (8), we see that,

at least asymptotically, the quantities

$$\varepsilon_2 = \varepsilon^0(\tilde{\omega})^{1/2}\varepsilon^0(\tilde{\psi})^{1/2} \tag{10a}$$

$$\varepsilon_3 = \frac{1}{2\alpha}(\varepsilon^0(\tilde{\omega}) + \alpha^2\varepsilon^0(\tilde{\psi})) \tag{10b}$$

give upper bounds for $|\Phi - \tilde{\Phi}|$. From what we have said before, it can be seen that the extent of the asymptotic overestimation of $|\Phi - \tilde{\Phi}|$ by ε_2 is closely related to the angle γ. For γ near 0 degrees, ε_2 is asymptotically a very sharp estimate for $|\Phi - \tilde{\Phi}|$, whereas if γ is close to 90 degrees, ε_2 will be a considerable overestimate.

3.2 The numerical algorithm

Let us now briefly list some features of the algorithm that we mentioned in the Section 1:

1. Instead of only solving for $\tilde{\omega}$, solutions for both $\tilde{\omega}$ and $\tilde{\psi}$ are calculated. This is not as laborious as it may at first seem, since the auxiliary problem for ψ and the basic problem for ω differ only in their loading data. Thus, they may be thought of as the solutions of a multiple load problem.
2. The pair of solutions $\tilde{\omega}$ and $\tilde{\psi}$ are computed for a sequence of adaptively refined meshes using the FEARS program. The mesh refinement steps are based on the particular choice of error indicators

$$\eta_\Delta = \frac{1}{2\alpha}(\eta^0(\tilde{\omega}) + \alpha^2\eta^0_\Delta(\tilde{\psi})) \tag{11}$$

where $\alpha > 0$ is some user chosen constant. The choice (11) is obviously suggested by (8b), the logic being that with this choice the adaptive mesh refinement process is directed by an 'optimal' minimization of the estimate ε_3. Recall that asymptotically ε_3 is, in general, only an upper bound for $|\Phi - \tilde{\Phi}|$, the degree of overestimation being determined by, among other factors, the angle γ and the value of α. It would seem preferable to employ error indicators whose sum provided a sharper estimate than (8b). Unfortunately, the two other estimates ε_1 and ε_2 that we have available cannot be expressed in the form (1). In the case of ε_1, choosing $\eta_\Delta = \frac{1}{4}(\eta^0(\tilde{\omega} + \tilde{\psi}) - \eta^0_\Delta(\tilde{\omega} - \tilde{\psi}))$ would not always ensure that $\eta_\Delta \geq 0$. The estimate ε_2 cannot be conveniently written as an element-by-element sum, although by a proper choice of α the values of ε_2 and ε_3 can be made close. We shall say a little more about this later.
3. Although ε_1 and ε_2 cannot be used in the role described in paragraph 2, they can still nevertheless be computed as global quantities and be employed as *a posteriori* error estimates. As such, they provide a means of stopping the mesh refinement process once sufficient accuracy has been attained. Of course, ε_1 would provide a superior estimate to ε_2 as long as the above-mentioned loss of reliability associated with angles γ near the 90 degrees does not occur.

4 NUMERICAL EXAMPLES

4.1 The membrane examples in Section 5 of Reference 1

Let us reconsider the example that we first discussed in Section 5 of Reference 1. In that example we dealt with the boundary value problem

$$\begin{aligned} \nabla^2\omega &= -1 \quad \text{in } \Omega = (-1, 1)^2 \\ \omega &= 0 \quad \text{on the boundary } \partial\Omega \text{ of } \Omega \end{aligned} \tag{12}$$

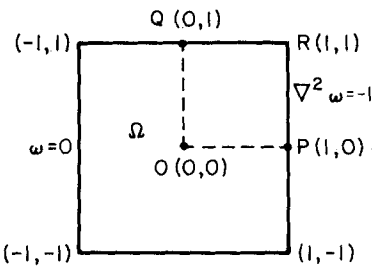

Figure 2. The region for the model problem (12)

One of our goals in that example was to find approximate values for the 'stress' $\Phi_2 = \partial\omega/\partial x_1$ at $P(1, 0)$ (see Figure 2). In Reference 1, we presented three different extraction expressions for this stress. These extraction expressions differed in the way that they handled the boundary conditions for the generating function. Here, we shall only further discuss the case (c) of Subsection 5.3 of Reference 1; that is, we consider post-processing calculations based on the extraction expression

$$\tilde{\Phi}_2(\tilde{\omega}) = \int_\Omega \nabla^2\phi\tilde{\omega}\, dA + \int_\Omega \phi\, dA \tag{13}$$

where

$$\phi = \frac{1}{\pi}\left[\frac{(x_1-1)}{(x_1-1)^2+x_2^2} - \left\{\frac{x_1-1}{(x_1-1)^2+1} + \frac{x_1-1}{4+x_2^2} - \frac{x_1-1}{5}\right\}\right]$$

The auxiliary problem associated with (13) is

$$\begin{aligned} \nabla^2\psi &= -\nabla^2\phi \quad \text{in } \Omega \\ \psi &= 0 \qquad\quad \text{on } \partial\Omega \end{aligned} \tag{14}$$

which, as it should be, is of the same form as (12) but with different right-hand sides.

In Reference 1, we saw that (13) led to highly accurate approximations for Φ_2, even in the case of quite coarse meshes. The numerical results we reported there were for a sequence of uniform meshes. At the time we did not comment on this particular selection of meshes. Qualitatively, however, such a choice would not seem unreasonable from the viewpoint of the theory we developed in References 1 and 2. The solutions of both the basic problem (12) and the auxiliary problem (14) are relatively smooth. Thus, uniform meshes would seem appropriate. In fact, the adaptive mesh refinement algorithm that we outlined in Subsection 3.2 exactly reproduces this sequence of meshes, independently of α.

Using the estimates given in Subsection 3.1, we are able to estimate the error in the post-processed value $\tilde{\Phi}_2$. For the above meshes, Table II lists a selection of *a posteriori* estimates for $|\Phi_2 - \tilde{\Phi}_2|$ based on (9) and (10). Notice that in the case of ε_1 the ratio of the estimated error to that true error in $\tilde{\Phi}_2$ appears to converge to 1 as the mesh size is decreased. This is consistent with (7). On the other hand, for ε_2 and ε_3 the corresponding ratios each seem to stabilize around values greater than 1 as the mesh is refined. Again, this is expected on the basis of (8), which shows that ε_2 and ε_3 will, in general, asymptote to upper bounds for the error. Let us also remark that since ε_2 gives only a slight overestimation of $|\Phi_2 - \tilde{\Phi}_2|$ and ε_1 behaves quite well, we should expect that the angle γ between $(\omega - \tilde{\omega})$ and $(\psi - \tilde{\psi})$ is not too close to 90 degrees. In Table II we have listed an estimate for this angle which confirms this expectation. Notice also the interesting fact that γ is almost independent of the mesh.

Table II. *A posteriori* estimates of the error in $\tilde{\Phi}_2$ for the example discussed in Subsection 4.1. $\varepsilon_1 = \frac{1}{4}|\varepsilon^0(\tilde{\omega}+\tilde{\psi}) - \varepsilon^0(\tilde{\omega}-\tilde{\psi})|$, $\varepsilon_2 = \varepsilon^0(\tilde{\omega})^{1/2}\varepsilon^0(\tilde{\psi})^{1/2}$, $\varepsilon_3 = \frac{1}{2}(\varepsilon^0(\tilde{\omega}) + \varepsilon^0(\tilde{\psi}))$

No. of elements in quarter segment (uniform mesh)	4	16	64
$\left\|\Phi_2 - \frac{\partial\tilde{\omega}}{\partial x_1}(P)\right\| / \|\Phi_2\|$			
relative error in standard finite element stress value	29%	16%	8·7%
$\|\Phi_2 - \tilde{\Phi}_2\|$			
error in post-processed stress value	10·495 (−3)	2·553 (−3)	0·637 (−3)
$(\|\Phi_2 - \tilde{\Phi}_2\| / \|\Phi_2\|)$	(1·5%)	(0·37%)	(0·089%)
γ			
angle between $(\omega - \tilde{\omega})$ and $(\psi - \tilde{\psi})$ (see equation (6))	37·1°	37·0°	38·6°
ε_j			
estimated error			
$(\varepsilon_j / \|\Phi_2 - \tilde{\Phi}_2\|)$			
ε_1	10·351 (−3) (0·986)	2·599 (−3) (1·018)	0·641 (−3) (1·006)
ε_2	12·976 (−3) (1·236)	3·255 (−3) (1·275)	0·820 (−3) (1·287)
ε_3	24·412 (−3) (2·326)	6·444 (−3) (2·524)	1·689 (−3) (2·651)

4.2 The slit membrane example in Subsection 6.2 of Reference 2

In this section we shall return to Example A in Section 6 of Reference 2. We have already used this example in Section 2 of this paper to illustrate some of the features of the FEARS program. The governing equations and boundary conditions are given in (2) and depicted in Figure 1. As in Reference 2, let us be interested in using post-processing techniques to find approximations to the leading stress intensity factor k_1. Recall that k_1 was defined to be the coefficient of the leading term in the asymptotic expansion

$$\omega = k_1 r^{1/4} \sin\frac{\theta}{4} + O(r^{3/4}) \qquad (k_1 = 1{\cdot}35812) \tag{15}$$

for ω in the vicinity of the slit tip $(0, 0)$. Here, we shall only treat post-processing calculations based upon the extraction expression

$$\tilde{k}_1 = \int_{\Gamma_3} (x_2\phi - \nabla\phi \,.\, \hat{n}\tilde{\omega})\, \mathrm{d}s \tag{16}$$

where

$$\phi = \frac{2}{\pi} r^{-1/4} \sin\frac{\theta}{4}$$

Expression (16) is an instance of what we have been calling a generalized influence function method. The auxiliary function introduced in the error analysis of the extraction expression (16) is

$$\begin{aligned} \nabla^2\psi &= 0 && \text{in } \Omega \\ \psi &= 0 && \text{on } \Gamma_1 \\ \frac{\partial\psi}{\partial n} &= 0 && \text{on } \Gamma_2 \\ \frac{\partial\psi}{\partial n} &= -\frac{\partial\phi}{\partial n} && \text{on } \Gamma_3 \end{aligned} \tag{17}$$

By chance, in this case, we can explicitly solve (17) to obtain

$$\psi = \frac{2}{\pi} r^{1/4} \sin\frac{\theta}{4} \tag{18}$$

which is just a multiple of the leading term in the expansion (15) of ω. (Of course, we cannot expect to be able to do this so simply in general.)

As explained in Section 2, the meshes we considered there and in Reference 2 for this problem were constructed by FEARS using the error indicator $\eta_\Delta = \eta_\Delta^0(\tilde{\omega})$. (That is, on the basis of minimizing the estimate ε^0 of the strain energy $E(\omega - \tilde{\omega})$ of the error.) Strictly speaking, this indicator does not fit into the framework we outlined in paragraph 2 of Subsection 3.2, although it can be thought of as a limiting case as $\alpha \to 0$. However, executing the algorithm of Subsection 3.2 with a number of choices of α leads to sequences of meshes which, although different from those above, show much the same refinement characteristics. For this reason, and since we want our numerical results here to complement those of Reference 2, we shall work with the same sequence of meshes constructed for this problem in Reference 2.

To try to see why the character of the meshes constructed above should be independent of α let us rewirte (15) as

$$\begin{aligned} \omega &= k_1 r^{1/4} \sin\frac{\theta}{4} + \omega_0 \\ &= k_1 \frac{\pi}{2} \psi + \omega_0 \end{aligned} \tag{19}$$

where $\omega_0 = O(r^{3/4})$. Let $\tilde{\omega}_0$ be the finite element solution that would be obtained were the loading in (2) such that ω_0 was the exact solution. By the linearity of the model problem,

$$\tilde{\omega} = k_1 \frac{\pi}{2} \tilde{\psi} + \tilde{\omega}_0$$

and consequently

$$\omega - \tilde{\omega} = k_1 \frac{\pi}{2} (\psi - \tilde{\psi}) + \omega_0 - \tilde{\omega}_0 \tag{20}$$

The function ω_0 is relatively smooth in comparison with ψ; however, from our point of view the relative magnitude of the factor $k_1\ \pi/2$ is equally important. If it is sufficiently large, then $k_1\ \pi/2(\psi - \tilde{\psi})$ will make the major contribution to the error $\omega - \tilde{\omega}$; while if it is small enough, then for meshes that are not too fine, the $\omega_0 - \tilde{\omega}_0$ contribution will dominate. As long as the first case applies, then an 'ideal' finite element mesh would exhibit a severe refinement about

the slit tip at (0, 0), whereas if the latter case applies, a more uniform mesh is called for, at least to begin with. Which case actually occurs in this problem is clearly demonstrated by the results shown in Table III—for the level of refinement encountered there, the $\omega_0 - \tilde{\omega}_0$ contribution is relatively small. It is not surprising then, that regardless of whether the mesh refinement process is directed towards minimizing $E(\omega - \tilde{\omega})$, $E(\psi - \tilde{\psi})$ or some combination $E(\omega - \tilde{\omega}) + \alpha^2 E(\psi - \tilde{\psi})$, the resulting meshes will not be significantly different. However, we should point out, and the trend in Table III shows this, that at some point the magnitude of the two components in (20) will become comparable. At that point, the different choices of α will lead to meshes of significantly different natures.

Table III. Magnitude of the $k_1(\pi/2)(\psi - \tilde{\psi})$ and $(\omega_0 - \tilde{\omega}_0)$ components of the error $(\omega - \tilde{\omega})$

Mesh label	$\dfrac{\lvert k_1(\pi/2)E(\psi - \tilde{\psi})^{1/2}}{E(\omega - \tilde{\omega})^{1/2}}$	$\dfrac{E(\omega_0 - \tilde{\omega})^{1/2}}{E(\omega - \tilde{\omega})^{1/2}}$
I	0·98	0·21
II	1·02	0·22
III	0·99	0·25
IV	0·96	0·34
V	0·94	0·38

In Table IV we list a number of different *a posteriori* estimates of the error in $\tilde{k}_1$ for the above sequence of meshes, along with the exact values of the error and the angle γ which are able to be found analytically for this particular problem. The apparent asymptotic exactness of ε_1 is consistent with (7) and the fact that the angle γ is rather small. The estimates ε_2 and ε_3 appear to lead to upper bounds for $|k_1 - \tilde{k}_1|$. Since the angle γ is near 0 degrees we would expect that ε_2 would, in the limit, give only a slight overestimation of the error. Again the numerical results in Table IV are consistent with this.

4.3 A modification of the slit membrane example in Subsection 6.2 of Reference 2

Let us now alter the basic problem (2) that we have been considering in Section 4.2 by modifying the loading so as to reduce the leading stress intensity factor by an order of magnitude or so. Specifically, in place of (2) consider

$$\begin{aligned} \nabla^2 \omega^* &= 0 \quad \text{in } \Omega \\ \omega^* &= 0 \quad \text{on } \Gamma_1 \\ \frac{\partial \omega^*}{\partial n} &= 0 \quad \text{on } \Gamma_2 \\ \frac{\partial \omega^*}{\partial n} &= x_2 + \frac{1}{4}\left(1{\cdot}3 \sin\frac{\theta}{4}\right) \quad \text{on } \Gamma_3 \end{aligned} \tag{21}$$

which has the exact solution $\omega^* = \omega + 1{\cdot}3 r^{1/4} \sin \theta/4$, where ω is the solution of (2). The leading stress intensity factor for ω^* is

$$k_1^* = k_1 + 1{\cdot}3 = -0{\cdot}058122$$

Table IV. *A posteriori* error estimates for $|k_1-\tilde{k}_1|$ for the example of Subsection 4.2. $\varepsilon_1 = \frac{1}{4}|\varepsilon^0(\tilde{\omega}+\tilde{\psi})-\varepsilon^0(\tilde{\omega}-\tilde{\psi})|$, $\varepsilon_2 = \varepsilon^0(\tilde{\omega})^{1/2}\varepsilon^0(\tilde{\psi})^{1/2}$, $\varepsilon_3 = \frac{1}{2}(\varepsilon^0(\tilde{\omega})+\varepsilon^0(\tilde{\psi}))$

Mesh label (degrees-of-freedom)	I (56)	II (89)	III (118)	IV (171)	V (391)
$\lvert k_1-\tilde{k}_1\rvert$ error in post-processed stress intensity factor	0·193860	0·123570	0·067090	0·029140	0·010690
$(\lvert k_1-\tilde{k}_1\rvert/\lvert k_1\rvert)$	(14·3%)	(9·1%)	(4·9%)	(2·1%)	(0·79%)
γ angle between $(\omega-\tilde{\omega})$ and $(\psi-\tilde{\psi})$ (see equation (6))	12·0°	12·5°	14·6°	20·1°	22·4°
ε_j estimated error					
$(\varepsilon_j/\lvert k_1-\tilde{k}_1\rvert)$					
ε_1	0·054270	0·055086	0·039720	0·022281	0·010163
	(0·28)	(0·45)	(0·59)	(0·76)	(0·95)
ε_2	0·059839	0·059906	0·043795	0·025825	0·011576
	(0·31)	(0·48)	(0·65)	(0·89)	(1·08)
ε_3	0·082962	0·077077	0·058214	0·035249	0·015912
	(0·43)	(0·62)	(0·87)	(1·21)	(1·49)

The algorithm in Subsection 3.2 was executed for this problem with the following three different choices of error indicator η_Δ of (11) governing the mesh construction process:

A. $\eta_\Delta = \eta_\Delta^0(\tilde{\omega}^*)$. (This can be thought of as a limiting form of (11) as $\alpha \to 0$, the normalizing factor $1/2\alpha$ of (11) having no effect on the refinement process.)
B. $\eta_\Delta = \sqrt{5}/2(\eta_\Delta^0(\tilde{\omega}^*)+\frac{1}{5}\eta_\Delta^0(\tilde{\psi}))$.
C. $\eta_\Delta = \eta_\Delta^0(\tilde{\psi})$. (This can be thought as a limiting form of (11) as $\alpha \to \infty$.)

Some numerical results for a selection of meshes obtained using each of these indicators is reported in Table V. The first thing to notice from Table V are the very significant differences between the meshes created using each of the above three indicators. As the 'distribution of elements' columns show, strategy C leads to meshes that concentrate elements in the inner subregions near the slit tip, while B and A produce progressively less severe refinement. This effect can be readily explained, as follows. In place of (20) we now have

$$\omega^*-\tilde{\omega}^* = k_1^*\frac{\pi}{2}(\psi-\tilde{\psi})+(\omega_0-\tilde{\omega}_0) \tag{22}$$

and, since $|k_1^*|$ is now significantly smaller than $|k_1|$, we can no longer regard the $(\omega_0-\tilde{\omega}_0)$ contribution to the error as negligible, as we could in Subsection 4.2. Indeed, for the initial uniform mesh I^*, from which each of our strategies A, B and C starts,

$$\frac{|k_1^*-\pi/2|E(\psi-\tilde{\psi})^{1/2}}{E(\omega^*-\tilde{\omega}^*)^{1/2}} = 0{\cdot}20 \quad \text{and} \quad \frac{E(\omega_0-\tilde{\omega}_0)^{1/2}}{E(\omega^*-\tilde{\omega}^*)^{1/2}} = 0{\cdot}98$$

Table V. Properties of meshes for (21), refined using strategies A, B and C (see text for details). Columns headed 'Distribution of elements' list percentage of elements in subregions 9–12 (inner) and 1–8 (outer), see Figure 1; d-o-f = degrees-of-freedom;

$$\Delta_A = \left(\frac{E(\omega^* - \tilde{\omega}^*)}{E(\omega^*)}\right)^{1/2} \qquad \Delta_B = \left(\frac{E(\omega^* - \tilde{\omega}^*) + \frac{1}{5}E(\psi - \psi^*)}{E(\omega^*) + \frac{1}{5}E(\psi)}\right)^{1/2} \qquad \Delta_C = \left(\frac{E(\psi - \tilde{\psi})}{E(\psi)}\right)^{1/2}$$

Mesh label	No. of elements	No. of d-o-f	Distribution of elements: inner	Distribution of elements: outer	Δ_A	Δ_B	Δ_C	$\left\|\frac{k_1^* - \tilde{k}_1^*}{k_1^*}\right\|$
I*:								
(Initial uniform mesh)	48	46	25%	75%	7·98%	11·0%	53·4%	14·4%
II*:								
Strategy A, II_A^*	108	109	48%	52%	5·52%	8·53%	46·1%	4·22%
Strategy B, II_B^*	123	117	55%	45%	5·08%	7·87%	42·5%	3·85%
Strategy C, II_C^*	108	102	70%	30%	5·89%	7·78%	36·2%	3·15%
III*:								
Strategy A, III_A^*	339	330	45%	55%	2·37%	4·95%	30·6%	2·87%
Strategy B, III_B^*	369	339	60%	40%	2·94%	4·03%	19·6%	1·23%
Strategy C, III_C^*	396	323	92%	8%	5·42%	5·78%	15·2%	1·30%

which is almost an exact reversal of the situation for mesh I in Subsection 4.2 (see Table III). Therefore, it is to be expected that strategy A, which seeks to minimize $E(\omega^* - \tilde{\omega}^*)$; strategy B, which seeks to minimize $(\sqrt{5}/2)(E(\omega^* - \tilde{\omega}^*) + \frac{1}{5}E(\psi - \tilde{\psi}))$; and strategy C, which seeks to minimize $E(\psi - \psi^*)$, will now lead to meshes that are of a quite different nature from the very start. The meshes produced by C should exhibit the severest refinement, reflecting the fact that such a refinement is necessary to approximate the singular function ψ well. On the other hand, A should produce the most uniform-like mesh since, early on, the smooth component $\omega_0 - \tilde{\omega}_0$ dominates the error $(\omega^* - \tilde{\omega}^*)$, and uniform-like meshes are sufficient to approximate ω_0 well. The actual meshes produced are in accord with these expectations.

Notice also that the meshes produced by the algorithm seem to have achieved their respective goals in some 'optimal' fashion, at least in comparison to one another. Among the meshes III_A^*, III_B^* and III_C^*, each of which has a comparable number of degrees-of-freedom, the mesh III_A^* has the lowest value for $E(\omega^* - \tilde{\omega}^*)$ (see column headed Δ_A), the mesh III_B^* has the lowest value for $(\sqrt{5}/2)(E(\omega^* - \tilde{\omega}^*) + \frac{1}{5}E(\psi - \psi^*))$ (see column headed Δ_B), while the mesh III_C^* has the smallest energy error in $(\psi - \tilde{\psi})$ (see column headed Δ_C).

Let us now turn to the accuracy in the post-processed value $\tilde{k}_1^*$ for the various meshes. As we have said previously, this accuracy is dependent not only on the accuracy of $\tilde{\omega}^*$, but also on the accuracy of $\tilde{\psi}$. Referring to Table V, we see that the meshes II_A^* and III_A^*, although yielding good accuracies for $\tilde{\omega}^*$ in the energy, are the worst members from among the sets II* and III*, respectively, as far as the accuracy of $\tilde{\psi}^*$ in energy is concerned. Not surprisingly then, the accuracy of $\tilde{k}_1^*$ for the meshes II_A^* and III_A^* is inferior to that for the corresponding meshes constructed using strategies B and C. The question obviously arises as to what is the choice of α for use in (11) that gives the best accuracy in k_1^* for a given number of degrees-of-freedom. This is a difficult matter to analyse in detail, although the results of Table V seem to indicate that, at least for this problem, the results are rather insensitive to non-zero choices of α. As a rough guide, however, and this is how we chose our $\alpha = 1/\sqrt{5}$, α could be selected

so that, for the initial uniform mesh, $\varepsilon^0(\tilde{\omega}^*)$ and $\alpha^2\varepsilon^0(\tilde{\psi})$ are about equal. The logic behind this choice is that this α approximately equalizes ε_3 and the asymptotically sharper estimate ε_2 (at least for the initial uniform mesh). Although we had no need to do so in our calculations, one could possibly change α during the course of the calculations to ensure that ε_3 and ε_2 always remain close to one another.

Finally, let us say a little about the *a posteriori* estimates for $|k_1^* - \tilde{k}_1^*|$ based upon ε_1, ε_2 and ε_3. Some numerical results for the mesh sequence I*, II_B^* and III_B^* are reported in Table VI. We also list the value of the angle γ between the errors $(\omega^* - \tilde{\omega}^*)$ and $(\psi - \tilde{\psi})$. For this problem, we are able to calculate γ exactly. Notice that these angles are rather close to the critical value $\gamma = 90$ degrees. As we explained in Subsection 3.1, for such values of γ we expect the estimate ε_1 to be unreliable due to the significance of the second term of (7). In addition, the estimate ε_2 should be a considerable overestimation of $|k_1^* - \tilde{k}_1^*|$. Our numerical results seem to confirm both these points.

Table VI. *A posteriori* estimates for $|k_1^* - \tilde{k}_1^*|$ for the example of Subsection 4.3

$\varepsilon_1 = \frac{1}{4}|\varepsilon^0(\tilde{\omega}^* + \tilde{\psi}) - \varepsilon^0(\tilde{\omega}^* - \tilde{\psi})|$ $\quad \varepsilon_2 = \varepsilon^0(\tilde{\omega}^*)^{1/2}\varepsilon^0(\tilde{\psi})$ $\quad \varepsilon_3 = \sqrt{(5/2)}(\varepsilon^0(\tilde{\omega}^*) + \frac{1}{5}\varepsilon^0(\tilde{\psi}))$

Mesh label (degrees-of-freedom)	I* (56)	II_B^* (117)	III_B^* (339)
$\lvert k_1^* - \tilde{k}_1^* \rvert$ error in post-processed stress intensity factor	0·8357 (−2)	0·2239 (−2)	0·0717 (−2)
$\lvert(k_1^* - \tilde{k}_1^*\rvert/\lvert k_1^*\rvert)$	(14·4%)	(3·85%)	(1·23%)
γ angle between $(\omega^* - \tilde{\omega}^*)$ and $(\psi - \tilde{\psi})$ (see equation (6))	78·5°	84·0°	82·8°
ε_j estimated error			
$(\varepsilon_j/\lvert k_1^* - \tilde{k}_1^*\rvert)$			
ε_1	0·2360 (−2) (0·28)	0·1566 (−2) (0·70)	0·0103 (−2) (0·14)
ε_2	1·7513 (−2) (2·10)	1·4005 (−2) (6·26)	0·5170 (−2) (7·21)
ε_3	1·9150 (−2) (2·29)	1·4042 (−2) (6·27)	0·5174 (−2) (7·22)

In general, of course, we cannot calculate γ, and so in a case such as the above we could, just on the basis of ε_1, be deceived into believing that there is greater accuracy in $\tilde{k}_1^*$ than is actually the case. However, the fact that ε_1 and ε_2 differ by an order of magnitude or so should act as a warning that we are more likely in a near critical case. (In fact, the ratio $\varepsilon_1/\varepsilon_2$ is an estimate for $\cos\gamma$.) In such a situation, ε_1 should not be trusted, while ε_2 could be used to gauge the accuracy of $\tilde{k}_1^*$, realizing, however, that it is probably a considerable overestimation of the error.

5 CONCLUSIONS

Our main intention in this paper was to examine the behaviour of the algorithm of Subsection 3.2 in some model post-processing applications, concentrating especially on the mesh selection and error estimation features of the algorithm. As far as accuracy of the post-processed value was concerned, the particular examples dealt with here proved rather insensitive to the choice of α in the error indicator (11). In our most extreme example, the spread in accuracy for the same number of degrees-of-freedom was only by a factor of 2. Whether this insensitivity is a property to be expected in general is an open question at the moment. However, we can at least say, from a theoretical point of view, that some dependence on α is to be expected whenever the basic and auxiliary problems have solutions with different 'smoothness' characteristics.

Our examples also show that, except for the critical case when γ is near 90 degrees, the error estimates ε_1 and ε_2 perform well asymptotically. The occurrence of the critical case can be detected numerically by the fact that $\varepsilon_2/\varepsilon_1 \geq 5$, say. In this critical case, even though ε_1 appears unreliable, ε_2 still seems to provide a usable estimate, albeit an over-pessimistic one.

REFERENCES

1. I. Babuška and A. Miller, 'The post-processing approach in the finite element method—part 1: calculation of displacements, stresses and other higher derivatives of the displacements', *Int. j. numer. methods eng.* **20**, 1085–1109 (1984).
2. I. Babuška and A. Miller, 'The post-processing approach in the finite element method—Part 2: the calculation of stress intensity factors', *Int. j. numer. methods eng.* **20**, 1111–1129 (1984).
3. C. Mesztenyi and W. Szymczak, 'FEARS User's Manual', *Technical Note No. BN-991*, Inst. for Physical Science and Technology, Univ. of Maryland (1982).